

Surface termination of hematite at environmental oxygen pressures: Experimental surface phase diagram

A. Barbier,¹ A. Stierle,² N. Kasper,² M.-J. Guittet,¹ and J. Jupille³¹CEA-Saclay, DSM/DRECAM/SPCSI, 91191 Gif-Sur-Yvette, France²Max-Planck-Institut für Metallforschung, Heisenbergstrasse 3, D-70569 Stuttgart, Germany³INSP, Université Pierre et Marie Curie-Paris 6, and Université Denis Diderot-Paris 7, CNRS, UMR 7588, Campus Boucicaut, 140 rue de Lourmel, 75015 Paris, France

(Received 29 March 2007; published 14 June 2007)

We provide an experimental surface phase diagram (surface termination versus chemical oxygen potential) of α -Fe₂O₃(0001) using a natural single crystal surface. In a partial reduction reoxidation cycle, we observe a sequence from oxygen-, to ferryl-, and again oxygen-terminated surfaces, in better agreement with recent density functional theory in the generalized gradient approximation calculations than with calculations taking into account on-site Fe 3*d* Coulomb repulsion. The nonreversible change in surface termination is accompanied by the formation of basal twins, which act as a sink for the extra Fe ions during the surface transformation processes.

DOI: 10.1103/PhysRevB.75.233406

PACS number(s): 68.47.Gh, 75.50.Ee, 75.70.Rf, 78.70.Ck

Iron oxides belong to the most abundant minerals on Earth,¹ existing with a large variety of phases with different stoichiometries, structures, and magnetic properties.^{2–4} The growth of hematite (α -Fe₂O₃), the thermodynamically most stable iron oxide phase,⁵ in the form of chemically pure, natural single crystals is by itself an intriguing phenomenon. It takes place by the dehydration of goethite⁶ (α -FeOOH) at elevated temperatures, forming in water based solutions. As a consequence, the occurrence of hematite on Mars was stressed to indicate the presence of water.⁷ Hematite surfaces used in various conditions are involved in many applications, such as oxidation catalysts,⁸ gas sensors,⁹ sorbents,^{10,11} or in magnetic storage media as a pinning layer for spin valves.¹² It is, therefore, of utmost importance to investigate these surfaces under environmental conditions as a function of the oxygen pressure *p* and temperature *T* (defining the oxygen chemical potential¹³ μ).

Different stable (0001) terminations are predicted for hematite (bulk structure in Fig. 1) as a function of μ by combined density functional theory (DFT) and thermodynamics approach,^{8,14,15} using either the generalized gradient approximation^{8,14,15} (GGA) or a GGA+*U* approach,¹⁴ which includes a correction term *U* for the on-site Coulomb repulsion of the localized Fe 3*d* electrons to better account for electronic correlations.¹⁶ Upon decreasing μ , three surface structures are predicted to appear in the following order: bulklike oxygen-terminated O₃—Fe—,¹⁷ ferryl termination in which one double bonded Fe=O group is present per surface unit cell, and, finally, single and double Fe ion terminations competing with the transformation to Fe₃O₄. If all approaches agree about Fe terminations at low μ , one among the above GGA calculations does not include the Fe=O termination.⁸ More importantly, the GGA+*U* approach¹⁴ conflicts with GGA calculations^{8,14,15} about the stability of the polar O₃—Fe— termination, which is a major component of the α -Fe₂O₃(0001) surface phase diagram. Those discrepancies about the determination of the *relative values of* μ (Ref. 18) highlight today's insufficient theoretical description of strongly correlated systems such as hematite. They call on experimental observations.

Experimentally, attempts to solve the problem of preparing Fe₂O₃(0001) surfaces consisted either in growing epitaxial thin films^{8,19–21} or in using sputtered-annealed-oxidized single crystal surfaces,^{22,23} though the characterization of the bulk structure might be uneasy. Such studies essentially revealed mixed surface terminations. Suggested terminations for Fe₂O₃(0001) thin films are Fe-terminated surfaces,^{8,19,20} which may coexist with either ferryl groups,²⁰ O terminations,⁸ or hydroxyl terminations.²¹ On sputtered-annealed-oxidized single crystal surfaces, evidences were given for a long-range ordering of domains assigned to FeO(111) and Fe₂O₃(0001).^{22,23} All these reports describe out of equilibrium multidomain surface configurations, in which most structural characterization is operated by scanning tunneling microscopy measurements. Beyond their discrepancies, they could hardly unravel the phase stability diagram of the α -Fe₂O₃(0001) surface, which is the key measurement enabling a direct comparison with theoretical models. Hence, the questions of (i) the direct structural characterization of the termination of a well-defined hematite crystal and of (ii) the changes of that termination over a wide range of μ are yet unchallenged.

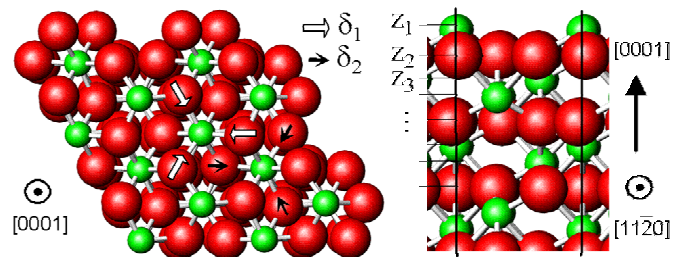


FIG. 1. (Color online) Schematic drawing of the α -Fe₂O₃(0001) structure. Large (small) circles stand for O (Fe) atoms. Top (left) and side (right) views with symmetry elements and allowed relaxations. Radial relaxations of the O atoms are labeled δ_i and relaxations of layer *i* along the [0001] axis by z_i .

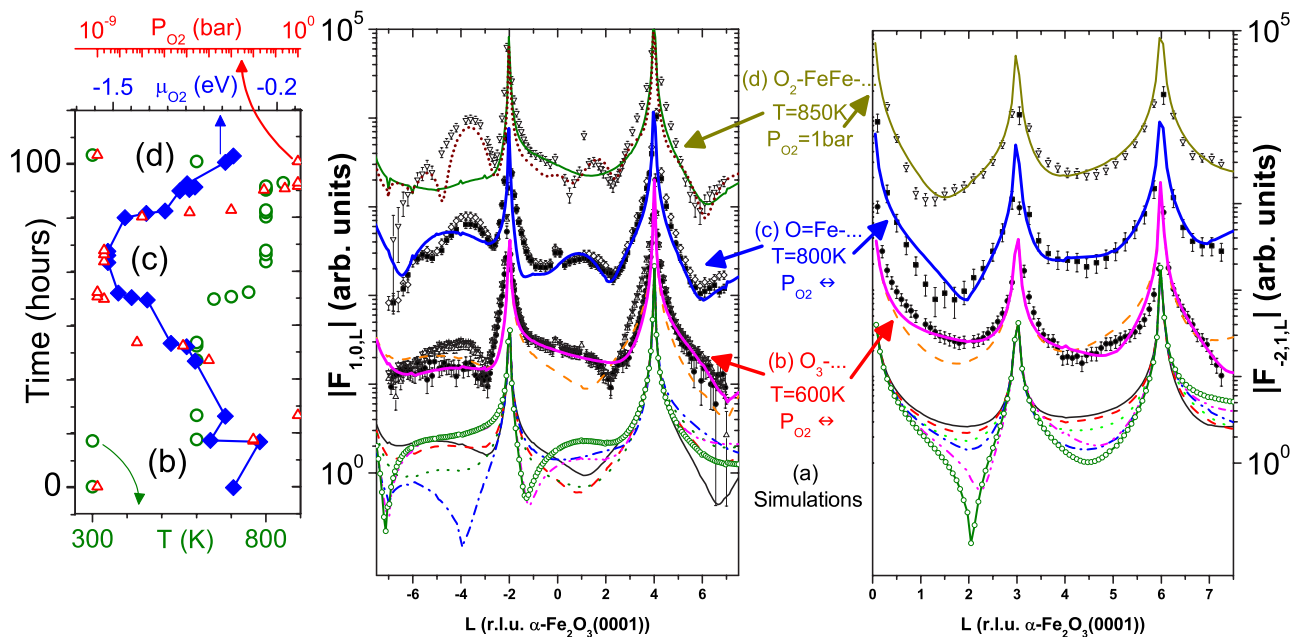


FIG. 2. (Color online) (Left panel) Temperature (T , \circ), oxygen pressure (P_{O_2} , Δ), and oxygen chemical potential (μ_{O_2} , \blacklozenge) as a function of time during the reduction-reoxidation experiment. (Right) $(10L)$ and $(\bar{2}1L)$ crystal truncation rods of $\alpha\text{-Fe}_2\text{O}_3(0001)$ for $300\text{ K} < T < 850\text{ K}$ and $6 \times 10^{-8}\text{ mbar} < P_{O_2} < 1\text{ bar}$. The L index describes the perpendicular momentum transfer [in reciprocal lattice units rlu of $\alpha\text{-Fe}_2\text{O}_3(0001)$]. Symbols represent structure factors. (a) Simulations using the surface terminations and relaxations from Ref. 15: (—) $O_3\text{—}$, (---) $O_2\text{—}$, (···) $O_1\text{—}$, (—○—) $Fe\text{—}O_3\text{—}$, (—○—) $O\text{=Fe—}$, and (—) $Fe\text{—}Fe\text{—}$. (b) (●) Outgassed surface (1 h, $T=573\text{ K}$, $P_{O_2}=10^{-5}\text{ mbar}$); annealing at $T=573\text{ K}$ with P_{O_2} decreasing from 10 mbar (∇) to $6 \times 10^{-8}\text{ mbar}$ (Δ); (—) x-ray refined best fit ($\chi^2 \sim 2$) to (●) considering an $O_3\text{—}$ surface termination; and (—) simulated rods for the $O_3\text{—}$ termination given in Ref. 14 within the GGA calculations. (c) $T=773\text{ K}$ with P_{O_2} increasing from $2 \times 10^{-6}\text{ mbar}$ (\blacksquare) to 1 mbar (∇); (—) best fit ($\chi^2 \sim 3$) to (\blacksquare) considering an $O\text{=Fe—}$ surface termination. (d) Annealing at $T=823\text{ K}$ (and measurement at 573 K) with $P_{O_2}=1\text{ bar}$ (∇); (—) best fit ($\chi^2 \sim 4$) considering an $O_2\text{—}Fe\text{—}Fe\text{—}$ surface termination; (···) best fit including 30% of three layer high basal twins. The systematic error on the structure factor is estimated $\sim 10\%$. The real space models corresponding to the best fits are given in Fig. 3.

To deal with those issues, an *in situ* structural analysis of a hematite surface has been performed. The surface preparation problem is solved by the use of a naturally (0001) oriented $\alpha\text{-Fe}_2\text{O}_3$ single crystal,²⁴ which does not require sputter-anneal cycles. The analysis is run by surface x-ray diffraction (SXR) on the six-circle diffractometer at the MPI-MF beamline at ANKA (Karlsruhe, Germany),²⁵ using a photon energy of 9.2 keV. The sample was mounted inside a high pressure cell (10^{-9} mbar–2 bar) equipped with a furnace (300–1000 K). The temperature was controlled by a thermocouple in direct contact with the sample. Hematite crystallizes in the hexagonal corundum structure (space group $R\bar{3}c$) with six formula units, and the following lattice parameters were used for the SXR experiment: $a=b=5.038\text{ \AA}$ and $c=13.772\text{ \AA}$.²⁶ X-ray photoemission spectra (XPS) only show lines characteristic of Fe, O, and C. To remove the carbon contamination, the surface is outgassed at $T=600\text{ K}$ under $P_{O_2}=10^{-5}\text{ mbar}$ for 1 h, which is an efficient cleaning procedure for air-exposed $\alpha\text{-Fe}_2\text{O}_3(0001)$ films and does not produce any phase change.²⁷ After the SXR experiment, XPS shows limited Na segregation, which is a much weaker x-ray scatterer as compared to Fe. Structural models including Na cannot explain our experimental observations. Finally, no evidence for surface reconstruction or decomposition have been observed during the experiment, which is confirmed by low energy electron dif-

fraction and XPS measurements performed after the SXR experiment.

Before discussing the experimental results, it is instructive to compare calculated crystal truncation rods (CTRs) for the different surface terminations as determined by theory. Two characteristic CTRs of the $\alpha\text{-Fe}_2\text{O}_3(0001)$ surface are shown in Fig. 2(a) and a large variation in the CTR amplitude is observed for different surface terminations.¹⁷ The CTR profile for a given surface termination agrees well for the different calculations.^{8,14,15} In addition, the $(10L)$ type CTRs are sensitive to the stacking of the metal ion planes and twin formation, whereas the $(\bar{2}1L)$ type CTRs are sensitive to the surface termination only.

To obtain the pure phase terminations of the $\alpha\text{-Fe}_2\text{O}_3(0001)$ surface, changes in the state of the surface were characterized by fast scans along the L direction. For selected, stable conditions, integrated intensities were measured by rocking scans with rotation axis normal to the surface ($\sim 150\text{--}200$ independent structure factors corrected for instrumental factors²⁸).

The CTRs measured after the initial cleaning procedure (573 K, $3 \times 10^{-5}\text{ mbar}$ O_2 pressure, and $\mu=-1\text{ eV}$) are reported in Fig. 2(b) (symbols). The overall shape of the rods is consistent with an $O_3\text{—}Fe\text{—}Fe$ surface termination since the theoretical $O_3\text{—}Fe\text{—}Fe$ relaxed surface models qualitatively reproduce the experimental data. In addition to the

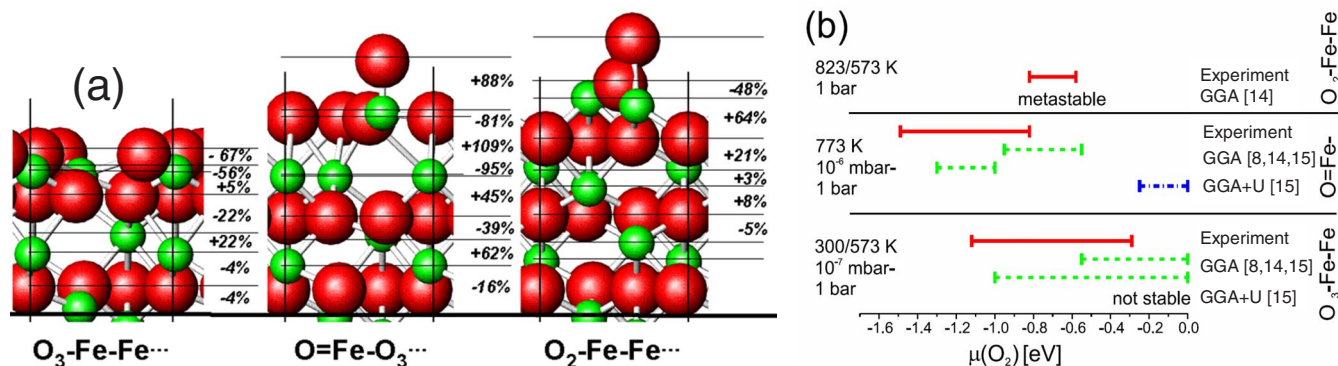


FIG. 3. (Color online) (a) $\alpha\text{-Fe}_2\text{O}_3(0001)$ stacking for the best fit structures obtained for $\text{O}_3\text{—}$, O=Fe— , and $\text{O}_2\text{—Fe—Fe}$ surface terminations. Large (small) circles stand for O (Fe) atoms. (b) Comparison of the experimental (solid lines) and theoretical stability regimes for the experimentally observed structures. The GGA calculations (dashed lines) show good agreement with the experimental stability regimes, whereas the GGA+ U calculation (dash-dotted line) does not. In the experiment, strong kinetic barriers exist and twin formation as an irreversible process takes place.

comparison with the theoretical models, a least-squares fitting procedure was used to obtain the best agreement with the data. The Debye-Waller factors and initial atomic positions were fixed to the bulk Fe_2O_3 values.²⁶ The high symmetry of the hematite structure strongly limits the possible structural relaxations (Fig. 1), since only two terminations are inequivalent with respect to the O_3 planes. The threefold axis lays on the Fe atoms, restricting to relaxations of Fe ions along the c axis. Oxygen atoms can undergo coplanar relaxations provided the unit cell keeps its threefold symmetry around the Fe sites.

The best fit yields $\delta_1 = -0.30$ Å and a surface roughness of ~ 4 Å. We find a strong contraction of the top interlayer distances, which is also a common feature of all theoretical models. In addition, the subsurface Fe ions form a nearly coplanar layer [see Fig. 3(a)]. After the refinement, the shortest fitted Fe—O bond is reduced by 8% relative to the theoretical models.¹⁵ The surface held at $T=573$ K is next exposed to decreasing $p(\text{O}_2)$ (Fig. 2) over a period of 48 h. The surface termination is hardly affected since the modest changes in the CTRs are limited to the $-6 < L < -3$ region of the $(10L)$ CTR.

However, increasing the temperature to $T=773$ K in the pressure range from 10^{-6} mbar to 1 bar leads to noticeable changes in the CTRs [Fig. 2(c)]. The strong reduction of the signal around $(10\bar{1})$ and $(\bar{2}12)$ is characteristic of a ferryl-terminated surface. Indeed, the O=Fe— model surface provides a better fit than the $\text{Fe—O}_3\text{—}$ single iron-terminated surface (χ^2 increases by a factor of 2). All other terminations can be ruled out, which further demonstrates that the ferryl termination is part of the oxygen/hematite (0001) phase diagram. The fit shown in Fig. 2(c) reveals $\delta_1 = -0.31$ Å and $\delta_2 = -0.01$ Å, and perpendicular relaxations are reported in Fig. 3. The topmost oxygen interlayer spacing is increased as compared to the bulk value by 88%, and the subsurface iron ions form a nearly coplanar layer similar to the $\text{O}_3\text{—Fe—Fe}$ terminated surface, in line with the DFT results.

Additionally, a peak develops on the $(10L)$ rod between $-6 < L < -3$. Its intensity increases systematically with annealing time and is insensitive to changes in the O_2 pressure.

The new peak likely arises from the formation of basal twins on the surface, since these are energetically favorable defects in corundum type materials.²⁹ The twin formation suggests a microscopic mechanism for the surface phase transformation from $\text{O}_3\text{—Fe—Fe}$ to O=Fe— : under oxidizing conditions, the extra Fe ions form Fe_2O_3 twin islands at the surface.

In a final step, the reversibility of the partial surface reduction was investigated by exposing the surface to 1 bar O_2 at 823 K [Fig. 2(d)]. The signal at $(\bar{2}12)$ is increasing again, in line with an oxygen surface termination [see Fig. 2(a)]. A good fit can be obtained for an $\text{O}_2\text{—Fe—Fe}$ model, as pictured in Fig. 3(a). The relaxations are in good agreement with those for a peroxide or dissociated O_2 structure of Ref. 15. The twin signal increases further and narrows, which imply that the lifting of the ferryl termination involves iron ion mass transport. In total, one double Fe layer was removed during the whole cycle, which is reflected quantitatively in the amount of twinned Fe_2O_3 that is formed. A good fit to the experimental data is obtained by including half a corundum unit cell thick twin islands, covering 30% of the surface [Fig. 2(d), dotted line]. The twin formation process is nonreversible as a function of the applied oxygen pressure and temperatures, which points to the high energetic stability of the twin grain boundaries.

The experimentally determined surface terminations and the corresponding p/T stability regions are summarized in Fig. 3(b). The observation of a stable oxygen terminated $\text{O}_3\text{—}$ surface over a wider range of oxygen chemical potential than in theoretical GGA predictions (the GGA+ U approach does not predict the $\text{O}_3\text{—}$ surface to be stable in the relevant μ regime) is most probably related to kinetic hindrance. The $\text{O}_3\text{—Fe}_3$ termination has not been observed, though it is expected to be slightly more stable than the $\text{O}_3\text{—}$ termination.¹⁴ The experimental finding of the formation of a ferryl O=Fe— termination in more reducing conditions ($\mu = -0.8$ eV to -1.5 eV) is in good agreement with the GGA results.^{14,15} When turning back to more oxidizing conditions, we cannot recover the $\text{O}_3\text{—}$ terminated surface. Instead, an $\text{O}_2\text{—Fe—Fe}$ terminated surface shows up. Since such terminations were predicted to be metastable in the DFT calculations from Ref. 15, the system might be trapped

by kinetic barriers. Down to $\mu = -1.5$ eV, no evidence was found for the formation of a single iron Fe—O₃ termination, though it is predicted below -0.95 eV in the GGA calculation^{14,15} or already below -0.25 eV in the GGA+ U approach.¹⁴ The whole process of partial reduction and re-oxidation is accompanied by the growth of basal twins. The formation of basal twin interfaces will also contribute to a reduction of the surface energy and has to be taken into account in the discussion of the surface energy.

In summary, we have determined the steady-state atomistic surface structures and phase stability domains of the (0001) surface of a hematite single crystal, a long-pending issue in surface and environmental science. The phase stability of the different terminations is in better agreement with the results from DFT-GGA calculations than with those of the DFT-GGA+ U approach, though the latter more accurately describes the bulk properties of hematite. Clearly, the energetics of the GGA+ U calculation does not agree with the experimentally observed μ stability regimes. This dis-

crepancy likely arises from correction parameter U for the on-site Coulomb repulsion of the localized Fe $3d$ electrons. A suggestion is that this parameter could vary from the bulk to the surface and from one termination to the next. In a partial reduction-reoxidation cycle, a sequence from oxygen-, to ferryl-, and again oxygen-terminated surfaces has been evidenced, in qualitative agreement with recent DFT studies. These different terminations may be exploited to produce surfaces with controlled chemical activity and magnetic properties for exchange coupling. Moreover, the stability of some of these structures against reoxidation shows that they might play a role in the surface properties of hematite, even in environmental conditions.

C. Speisser is gratefully acknowledged for providing the α -Fe₂O₃ single crystal. We thank H. Dosch for support and helpful discussions.

-
- ¹H. T. Dinh, J. Kuever, M. Mußmann, A. W. Hassel, M. Stratmann, and F. Widdel, *Nature (London)* **427**, 829 (2004).
²P. Kuiper, B. G. Searle, P. Rudolf, L. H. Tjeng, and C. T. Chen, *Phys. Rev. Lett.* **70**, 1549 (1993).
³Z. Zhang and S. Satpathy, *Phys. Rev. B* **44**, 13319 (1991).
⁴R. Pentcheva, F. Wendler, H. L. Meyerheim, W. Moritz, N. Jedrecy, and M. Scheffler, *Phys. Rev. Lett.* **94**, 126101 (2005).
⁵A. H. Morrish, *Canted Antiferromagnetism: Hematite* (World Scientific, Singapore, 1994).
⁶F. Watari, J. van Landuyt, P. Delavignette, S. Amelinckx, and N. Igata, *Phys. Status Solidi A* **73**, 215 (1982).
⁷G. Klingelhofer *et al.*, *Science* **306**, 1740 (2004).
⁸X.-G. Wang, W. Weiss, S. K. Shaikhutdinov, M. Ritter, M. Petersen, F. Wagner, R. Schlogl, and M. Scheffler, *Phys. Rev. Lett.* **81**, 1038 (1998).
⁹M. Ivanovskaya, D. Kotsikau, G. Faglia, P. Nelli, and S. Irkaev, *Sens. Actuators B* **93**, 422 (2003).
¹⁰T. Kendelewicz, P. Liu, C. S. Doyle, G. E. Brown, E. J. Nelson, and S. A. Chambers, *Surf. Sci.* **424**, 219 (1999).
¹¹B. V. Reddy and S. N. Khanna, *Phys. Rev. Lett.* **93**, 068301 (2004).
¹²C. Frandsen and S. Mørup, *Phys. Rev. Lett.* **94**, 027202 (2005).
¹³The oxygen chemical potential is related to the oxygen pressure p and the temperature T by $\mu = \mu_0(p_0, T) + \frac{1}{2}kT \ln(p/p_0)$, see Ref. 15 for details.
¹⁴A. Rohrbach, J. Hafner, and G. Kresse, *Phys. Rev. B* **70**, 125426 (2004).
¹⁵W. Bergermayer, H. Schweiger, and E. Wimmer, *Phys. Rev. B* **69**, 195409 (2004).
¹⁶G. Rollmann, A. Rohrbach, P. Entel, and J. Hafner, *Phys. Rev. B* **69**, 165107 (2004).
¹⁷A subscript number denotes the number of atoms in a layer in the unit cell, and the stacking from surface to bulk reads from left to right.
¹⁸ $\Delta\mu$ of about 0.8 eV, corresponding to an O₂ pressure difference of 12 orders of magnitude at 600 K.
¹⁹S. Chambers and S. I. Yi, *Surf. Sci. Lett.* **439**, L785 (1999).
²⁰C. Lemire, S. Bertarione, A. Zecchina, D. Scarano, A. Chaka, S. Shaikhutdinov, and H.-J. Freund, *Phys. Rev. Lett.* **94**, 166101 (2005).
²¹G. Ketteler, W. Weiss, and W. Ranke, *Surf. Rev. Lett.* **8**, 661 (2001).
²²Q. Guo, P. H. McBreen, and P. J. Møller, *Surf. Sci.* **423**, 19 (1999).
²³N. G. Condon, F. M. Leibsle, A. R. Lennie, P. W. Murray, D. J. Vaughan, and G. Thornton, *Phys. Rev. Lett.* **75**, 1961 (1995).
²⁴The crystal originating from Brazil had a surface of 6×15 mm² and an in-plane mosaic distribution of 0.01° characteristic for a perfect single crystal.
²⁵A. Stierle, A. Steinhäuser, A. Rühm, F. U. Renner, R. Weigel, N. Kasper, and H. Dosch, *Rev. Sci. Instrum.* **75**, 5302 (2004).
²⁶R. L. Blake, R. E. Hessevick, T. Zoltai, and L. W. Finger, *Am. Mineral.* **51**, 123 (1966).
²⁷A. Barbier, R. Belkhou, P. Ohresser, M. Gautier-Soyer, O. Bezenenet, M. Mulazzi, M.-J. Guittet, and J.-B. Moussy, *Phys. Rev. B* **72**, 245423 (2005).
²⁸E. Vlieg, *J. Appl. Crystallogr.* **30**, 532 (1986).
²⁹A. G. Marinopoulos, S. Nufer, and C. Elsässer, *Phys. Rev. B* **63**, 165112 (2001).